RSC Advances

PAPER

View Article Online
View Journal | View Issue

Cite this: *RSC Adv.*, 2014, **4**, 13093

Catalysis by metal–organic frameworks: proline and gold functionalized MOFs for the aldol and three-component coupling reactions†

Liu Lili,[a] Zhang Xin,*[a] Rang Shumin,[a] Yang Ying,[a] Dai Xiaoping,[a] Gao Jinsen,[a] Xu Chunming[a] and He Jing[b]

Translation of homogeneous catalysis into heterogeneous catalysis is a promising solution to green and sustainable development in the chemical industry. Recent research has shown that metal–organic frameworks (MOFs) could bridge the gap between homogeneous and heterogeneous catalysis. We successfully prepared for the first time a novel homochiral Zn-containing MOF referred to as CUP-1 based on the mixed linkers of 2-aminoterephthalic acid and L-lactic acid in a one-pot synthesis. The free NH_2 group in the homochiral framework of CUP-1, similar to the well known achiral IRMOF-3, is potentially available for undergoing a variety of organic transformations, as demonstrated by choosing the auxiliary chiral L-proline and nano gold to functionalize MOFs with postsynthetic modification and one-pot synthesis strategies. IRMOF-3, CUP-1 and their functionalized samples were in-depth characterized by X-ray diffraction, N_2 adsorption–desorption, optical and transmission electron microscopy, infrared spectroscopy, solid state nuclear magnetic resonance, thermogravimetric and differential thermal analysis, and temperature-programmed reduction. L-Proline functionalized IRMOF-3 shows fair to excellent enantioselectivity (up to 98%) in asymmetrical aldol reactions of aldehydes and acetone with higher turnover numbers and catalytic stabilities than the homogeneous counterpart. The gold functionalized CUP-1 catalysts are found to be highly active, stable and reusable for the three-component coupling reactions of aldehydes, alkynes and amines. This work provides general methods to functionalize MOFs with the active ligand and metal nanoparticles for fabrication of highly efficient MOF-based heterogeneous catalysts.

Received 13th February 2014
Accepted 25th February 2014

DOI: 10.1039/c4ra01269k

www.rsc.org/advances

1. Introduction

The challenge for green and sustainable development requires more efficient chemical transformations with less emission. With the development of catalytic transformations, chemists have found many efficacious methods to promote both step and atom economies in chemical syntheses. Among the catalytic pathways, both homogeneous and heterogeneous catalysis show advantages as well as pitfalls. Obviously, homogeneous catalysts are widely studied as powerful catalyst systems, owing to their unique properties such as designable structures, high catalytic activity and selectivity. However, homogeneous catalysts are usually difficult to separate from the reaction products since the catalysts are in the same phase as the reactants and products. While catalyst recovery and process work-up are much easier in the case of solid catalysts, it becomes more difficult to know the exact nature of the active sites. It is not then surprising that research efforts are being made today to bridge the gap between homogeneous and heterogeneous catalysis.[1]

Metal–organic frameworks (MOFs) are crystalline materials generated using metal ions or metal ion clusters that act as "nodes" combined with multidentate organic ligands to serve as "rods".[2–6] Unlike other materials (such as metal oxides), the unique properties such as high porosities, large surface areas, structural variety and considerable capacity to accommodate guest molecules, may provide the fully exposed active sites by anchoring them in proper position of the MOFs. Recent researches have shown that MOFs could bridge the gap between homogeneous and heterogeneous catalysis.[7–9] We noted that there are significantly increasing reports of chemical catalysis by MOFs in the past three years,[7–25] however, only two dozens of chiral MOFs with

[a]*State Key Laboratory of Heavy Oil Processing, China University of Petroleum, Changping, Beijing 102249, China. E-mail: zhangxin@cup.edu.cn; Fax: +86 10 8973 4979*

[b]*State Key Laboratory of Chemical Resource Engineering, Beijing University of Chemical Technology, Beijing 100029, China*

† Electronic supplementary information (ESI) available: Experimental section (reagents and chemicals and catalyst characterization), optical micrograph of the CUP-1 crystals (Fig. S1), mesopore diameter distribution determined by BJH desorption, TEM, GC-MS, selected bond lengths (Å) and crystal data for complexes Zn_2(atpt)(l-lac)(HCOO) (Tables S1–S3), HPLC traces and CUP-1.cif. CCDC 909362. For ESI and crystallographic data in CIF or other electronic format see DOI: 10.1039/c4ra01269k

catalytically active sites for asymmetrical catalysis have been reported to date.[5,17–25]

Metals and organic struts can act as active species for MOF-based asymmetrical catalysts.[6] This work has focused on creating catalytically active sites by introduction of active organic ligand (L-proline) and gold nanoparticles to fabricate solid MOF based catalysts. We have shown that the creation of catalytic active sites can be facially achieved by post modification (PM) and one-pot (OP) synthetic methods. We successfully synthesized a novel homochiral CUP-1 by the reaction of the mixed linkers of 2-aminoterephthalic (H_2atpt) acid and L-lactic acid with zinc nitrate. The homochiral CUP-1 entails free NH_2 groups, which does not participate in coordination to the pentanuclear Zn that linked the structure. The free NH_2 group in the homochiral framework of CUP-1, similar to the well known achiral IRMOF-3 is potentially available for undergoing a variety of organic transformations. It has been well documented that the post covalent modification of the NH_2 group of IRMOF-3 with several linear alkyl anhydrides, salicylaldehyde to introduce more complex functionality within the lattice.[7,26–29] In recent studies, Zhang *et al.* demonstrated that IRMOF-3 containing the Au(III) Schiff base complex can be lined the pore walls by PM method.[7] The extremely small (1.7 nm) gold nanoparticles on the surface of IRMOF-3 has also been reported with the OP synthesis.[30] We think that it is very interesting to functionalize CUP-1 and IRMOF-3 with the catalytic chiral reagent. L-Proline was chosen to functionalize CUP-1 and IRMOF-3 by PM and/or OP strategies, since L-proline and its derivatives are well-known asymmetrical organocatalysts accelerating a variety of enantioselective organic reactions under homogeneous conditions.[31,32] The asymmetrical aldol reaction of aldehyde and acetone and the three component coupling reaction of aldehyde, alkyne and amine (A^3) coupling reaction are chosen as the target reactions to demonstrate the catalytic properties of the L-proline and gold functionalized IRMOF-3 and CUP-1 catalysts. The interest of these reactions lies on the versatility of their products as synthetic intermediates in organic synthesis and as important therapeutic drug molecules.[30–32] These products are conventionally synthesized by using homogenous organometallic or purely organic catalysts with stoichiometric amounts under strictly controlled reaction conditions.

By immobilization of L-proline and gold nanoparticles into MOFs, we have developed green and sustainable heterogeneous catalysis for synthesis of β-hydroxy carbonyl compounds and propargylamines. L-Proline functionalized IRMOF-3 catalysts show fair to excellent enantioselectivity (up to 98%) in asymmetrical aldol reactions of aldehydes and acetone with higher turnover numbers and catalytic stabilities than the homogeneous counterpart.[31] The gold functionalized CUP-1 catalysts are found to be highly active, stable and reusable for the three-component coupling reactions of aldehyde, alkyne and amine. This work provides general methods to functionalize MOFs with the active ligand and metal nanoparticles for fabrication of highly efficient MOF-based catalysts.

2. Experimental

2.1. Catalyst preparation

2.1.1 Preparation of IRMOF-3. IRMOF-3 was synthesized and activated according to the procedure from literature[33,34] with slight modification. In a typical preparation, $Zn(NO_3)_2 \cdot 6H_2O$ (24.9 mmol) and H_2atpt (8.3 mmol) were dissolved in 200 mL DMF and stirred for 0.5 h at room temperature in air. The solution was transferred and sealed in a 500 mL teflon-lined autoclave, and kept at 100 °C for 18 h. The resulting brown solid was collected by centrifugation and washed thrice with DMF and $CHCl_3$ during three days, and the solid was finally dried in vacuum at 50 °C for 2 h.

2.1.2 Preparation of CUP-1. Typically, H_2atpt (0.5 mmol) and L-lactic acid (0.5 mmol) were dissolved in 10 mL DMF and stirred 0.5 h at room temperature in air. Then $Zn(NO_3)_2 \cdot 6H_2O$ (1 mmol) was added and continuingly stirred 0.5 h. The mixture was transferred and sealed in a teflon-lined stainless steel vessel for a certain time (24–48 h) at various temperatures (70–110 °C). The resulting brown solid was collected by centrifugation and washed thrice with DMF and ethylether during three days. The solid was finally dried in vacuum at 50 °C for 2 h.

2.1.3 Preparation of L-proline functionalized IRMOF-3 and CUP-1 catalysts. A solution of L-proline (18.3 mg) in ethanol (0.5 mL) was added dropwise to IRMOF-3 (0.2 g), and stored overnight at room temperature. The samples were dried in vacuum at 30 °C to yield IRMOF-3–Pr(PM). IRMOF-3–Pr(OP) was prepared by a mixture of $Zn(NO_3)_2 \cdot 6H_2O$ (1.0 mmol, 300 mg), H_2atpt (0.5 mmol, 93.0 mg), and L-proline (0.5 mmol, 57.5 mg) dissolved in 20 mL DMF and 20 mL ethanol. The mixture was heated in a teflon-lined steel vessel for 24 h at 100 °C. Then the yellow crystals were washed with DMF and $CHCl_3$ during three days, and the product was dried in vacuum at 30 °C. Specifically, IRMOF-3–Pr′(OP) were synthesized by using 0.25 mmol L-proline and a same procedure with IRMOF-3–Pr(OP).

For the synthesis of CUP-1–Pr(OP) by OP synthesis, the mixture of H_2atpt (0.5 mmol), L-lactic acid (0.5 mmol), and DMF (10 mL) was stirred for 0.5 h at room temperature. $Zn(NO_3)_2 \cdot 6H_2O$ (1.0 mmol) was added to the mixture and continuingly stirred for 0.5 h. Then a solution of L-proline (0.5 mmol) in ethanol (10 mL) was dropwise added. The mixture was transferred into a teflon-lined stainless steel vessel and heated for 48 h at 100 °C. The resulting yellow solid was collected by centrifugation and washed thrice with DMF and $CHCl_3$ during three days.

2.1.4 Preparation of gold functionalized CUP-1 catalysts. For the synthesis of gold functionalized CUP-1 by PM method, a solution of $NaAuCl_4 \cdot 2H_2O$ (0.045 g) in 0.3 mL MeCN was dropwise added to the CUP-1 (0.438 g) at room temperature and stored overnight. Then the sample was dried in vacuum at 30 °C for 2 h. The sample was referred to as Au/CUP-1(PM).

A typical procedure for preparing Au/CUP-1(OP) by OP method was following. A mixture of H_2atpt (0.5 mmol, 0.092 g), L-lactic acid (0.5 mmol, 0.045 g), and DMF (10 mL) were stirred for 0.5 h at room temperature. $Zn(NO_3)_2 \cdot 6H_2O$ (1.0 mmol, 0.300 g) was added to the mixture and continuingly stirred for 0.5 h.

Then a solution of AuCl (0.005 g) in DMF (1 mL) was dropwise added. The mixture was transferred into a teflon-lined stainless steel vessel and heated for 24 h at 110 °C. The resulting green solid was collected by centrifugation and washed thrice with DMF and $CHCl_3$. Then the sample was dried in vacuum at 30 °C for 2 h.

2.2. Catalytic performance

2.2.1 Asymmetrical aldol reaction of aldehyde with acetone. The mixture of benzaldehyde (0.3 mmol, 31.8 mg), acetone (3.0 mmol, 174.4 mg), DMSO (6.4 mmol, 0.5 g), and catalyst (20 mg) was put into a closed glass reactor (2 mL, SUPELCO) and extensively stirred (*ca.* 500 rpm) at a desired time and temperature. The amounts of active sites (*i.e.*, proline species) referred to benzaldehyde are 3.8, 9.2, and 14.6 mol% over IRMOF-3–Pr(OP), IRMOF-3–Pr(PM), and CUP-1–Pr(OP), respectively. After the reaction, the catalyst was removed from the solution by centrifugation at 6000 rpm for 10 minutes. The conversion of benzaldehyde and the yield of β-hydroxy carbonyl and α,β-unsaturated carbonyl compounds were determined by GC analysis (SP6890, Capillary Column, HP-5). And *n*-nonane was used as an internal standard. The product of β-hydroxy carbonyl compound was separated and purified by column chromatography on silica gel (EtOAc–hexane = 1/4 as the eluent). The ee values were determined by HPLC with a Chiralpak ID column, using hexane–2-propanol–diethylamine (80/20/0.1) as a mobile phase at a flow rate of 1.0 mL min^{-1} and a column temperature of 35 °C.

2.2.2 The A^3 coupling reaction. Typical procedure for the A^3 coupling reaction: a mixture of catalyst (0.070 g), benzaldehyde (0.250 mmol, 0.027 g), piperidine (0.300 mmol, 0.026 g), phenylacetylene (0.325 mmol, 0.034 g), and dioxane (1.000 g) was put into a closed glass reactor (2 mL, SUPELCO) and extensively stirred (*ca.* 500 rpm) at the desired time and temperature. The mole ratio of gold to benzaldehyde is 6.42 mol% and 0.14 mol% on Au/CUP-1(PM) and Au/CUP-1(OP), respectively. After the reaction, the catalyst was removed from the solution by centrifugation at 6000 rpm for 10 minutes. The product was analysed by GC (SP6890, Capillary Column, SE-30) and GC-MS. And *n*-nonane was used as an internal standard to calibrate the reaction products. The recovered catalyst was thoroughly washed with 1,4-dioxane and used for the next run. The ee values were determined by HPLC with a Chiralcel OD column, using hexane–ethanol (95/5) as a mobile phase at a flow rate of 0.5 mL min^{-1}. Before ee analysis, the product was purified with flash column chromatography on silica gel using the mixture of hexane and ethyl acetate (ethyl acetate = 15 vol%) as the eluent.

3. Results

3.1. Strategies for functionalization of IRMOF-3 and CUP-1

Scheme 1 illustrates our synthetic strategy to prepare the chiral MOF. The starting components are composed of H_2atpt, $Zn(NO_3)_2 \cdot 6H_2O$ and DMF. The hydrothermal reaction of these components in the mole ratio of 1 : 3 : 311 at 100 °C for 18 h afforded IRMOF-3 (Scheme 1a). By adding L-lactic acid to the starting components and hydrothermal heating at 100 °C for 48 h, a novel homochiral MOF referred to as CUP-1 was obtained (Scheme 1b). The introduction of auxiliary chiral L-proline unit inside preassembled framework of IRMOF-3 with PM method afforded IRMOF-3–Pr(PM) (Scheme 1c). In an alternative approach, L-proline was introduced with the starting components composed of IRMOF-3 or CUP-1 in a one-pot reaction to give IRMOF-3–Pr(OP) (Scheme 1e) or CUP-1–Pr(OP) (Scheme 1f). Specifically, gold functionalized CUP-1 with PM and OP methods afforded Au/CUP-1(PM) (Scheme 1d) and Au/CUP-1(OP) (Scheme 1g), respectively. Clearly the synthesis component for preparing IRMOF-3 is the same with CUP-1, except for the latter containing an additional chiral L-lactic acid. CUP-1 and IRMOF-3 and their functionalized catalysts have a close relationship in preparation procedures. According to the elemental analysis of the samples, 5.8, 3.2 and 7.4 wt% of L-proline was introduced in IRMOF-3–Pr(OP), IRMOF-3–Pr′(OP), and CUP-1–Pr(OP) samples, respectively. And 15.8 wt% of L-proline was introduced in IRMOF-3–Pr(PM). ICP-OES shows that the gold contents are 4.52 and 0.10 wt% on Au/CUP-1(PM) and Au/CUP-1(OP), respectively.

3.2. Optical micrographs and transmission electron microscope (TEM)

Fig. 1A gives the optical micrographs of IRMOF-3, IRMOF-3–Pr(OP), IRMOF-3–Pr′(OP), IRMOF-3–Pr(PM), CUP-1, and CUP-1–Pr(OP) samples. The IRMOF-3 structure[33,34] is made of Zn_4O tetranuclear clusters connected by rigid dicarboxylic linkers H_2atpt to generate a cubic framework as illustrated in Scheme 1a. IRMOF-3 exhibits a light brown cubic shape with sizes of 90–110 μm as illustrated in Fig. 1Aa. Using the auxiliary chiral L-proline to modify IRMOF-3 with OP method doesn't significantly affect the cubic crystal morphology for IRMOF-3–Pr(OP) (Fig. 1Ab), however, the size (30–80 μm) of cubic phase sharply decreased and very small cubic phase with *ca.* 10 μm was observed on IRMOF-3–Pr′(OP) (Fig. 1Ac). The modification of IRMOF-3 with L-proline by PM method resulted the fuzzy edge of IRMOF-3–Pr(PM) in despite of the discernable cubic morphology (Fig. 1Ad). CUP-1 with yellow plate crystals can be synthesized from the mixture of $Zn(NO_3)_2 \cdot 6H_2O$, H_2atpt, l-lac, DMF in a mole ratio of 2 : 1 : 1 : 258 as illustrated in Scheme 1b. We have studied the effect of crystallization temperature (70–110 °C) for CUP-1. It was found that heated at 70–100 °C for 24 h in a teflon-lined stainless-steel autoclave under autogeneous pressure there were no yellow plate products immerging, but amorphous substance (Fig. S1†). Extending the crystallization time from 24 to 48 h at 100 °C or increasing the reaction temperature to 110 °C for 24 h both achieved high quality plate crystals (Fig. 1Ae). It seems that crystallization temperature ranged from 100 to 110 °C has no significant effect on the crystal morphology of CUP-1 (Fig. S1†). Notably, the modification of CUP-1 with L-proline by OP method affects a spherical morphology (Fig. 1Af), which is sharply different from the plate crystal of CUP-1.

The representative TEM images of Au/CUP-1(PM) and Au/CUP-1(OP) samples are shown in Fig. 1B. Gold nanoparticles

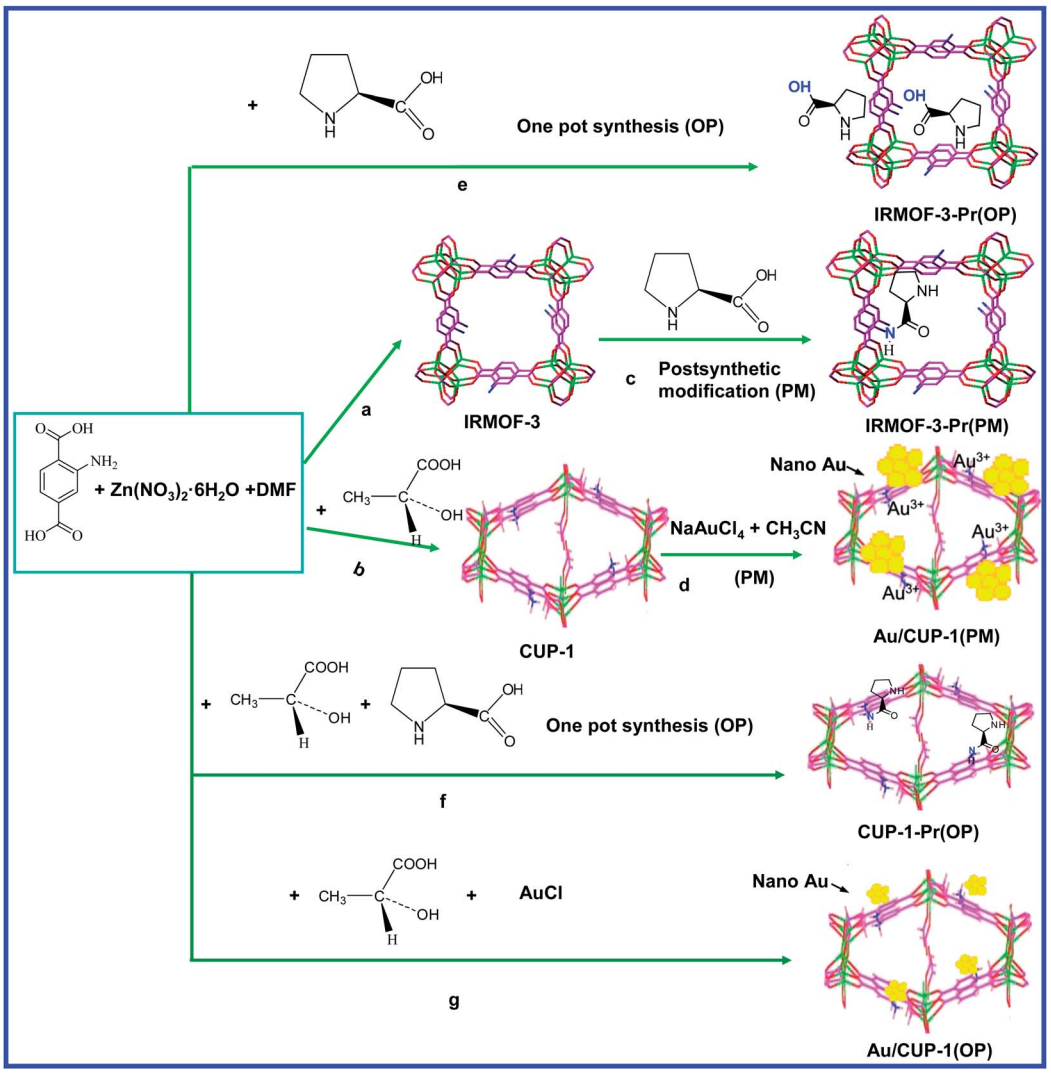

Scheme 1 The strategies and accordingly models for functionalizing IRMOF-3 and CUP-1 catalysts by postsynthetic modification (PM) and one-pot synthesis (OP).

are close to spherical morphology with size distributions of 13.9 ± 4.7 and 2.1 ± 0.7 nm over Au/CUP-1(PM) and Au/CUP-1(OP), respectively. After four successive cycles of the A^3 coupling reaction, both gold nanoparticles containing samples exhibited significant agglomeration. In the case of the recycled Au/CUP-1(OP) catalyst, the size distributions of gold particles range from 10 to 60 nm (Fig. S2†).

3.3. Powder X-ray diffraction (XRD)

Fig. 2A shows the powder XRD patterns of IRMOF-3 and its modified samples. XRD patterns of IRMOF-3–Pr(OP), IRMOF-3–Pr′(OP), and IRMOF-3 samples are nearly identical. The similar XRD patterns with IRMOF-3 indicate that IRMOF-3–Pr(OP) and IRMOF-3–Pr′(OP) samples keep the crystalline integrity. Although the peak intensities decreased on IRMOF-3–Pr(OP) after being used the aldol reaction at 60 °C for 72 h, the main diffraction peaks were retained. The XRD patterns of IRMOF-3–Pr(PM) show a difference with IRMOF-3, *i.e.*, the peak located at $2\theta = 6.8°$ disappears, indicating that the crystalline structure of IRMOF-3–Pr(PM) slightly changes. The result is in accordance with the observation of optical micrographs.

Fig. 2B shows the powder XRD patterns of CUP-1 and gold or L-proline functionalized CUP-1 samples. The theoretical simulated framework of CUP-1 from the structure solved by single-crystal XRD is also included. Clearly, the powder XRD patterns of CUP-1 give the high crystallinity and match very well with the theoretical patterns. Notably CUP-1 displays a similar XRD pattern with a homochiral MOF Zn_2(bdc)(l-lac)(dmf)·(DMF) (**1**·DMF).[5] The gold functionalized CUP-1 catalysts by PM and OP methods retain the crystalline structure. Notably, three additional peaks at $2\theta = 38.2°$, 44.4°, and 64.5° are observed for Au/CUP-1(PM), which are indexed to the (111), (200), and (220) reflections of face centered cubic crystalline Au, respectively. The average diameter of gold crystal was 12.5 nm calculated by Scherrer formula, which coincided with the observations from the TEM images. Similar to IRMOF-3–Pr(OP), the crystallinity of

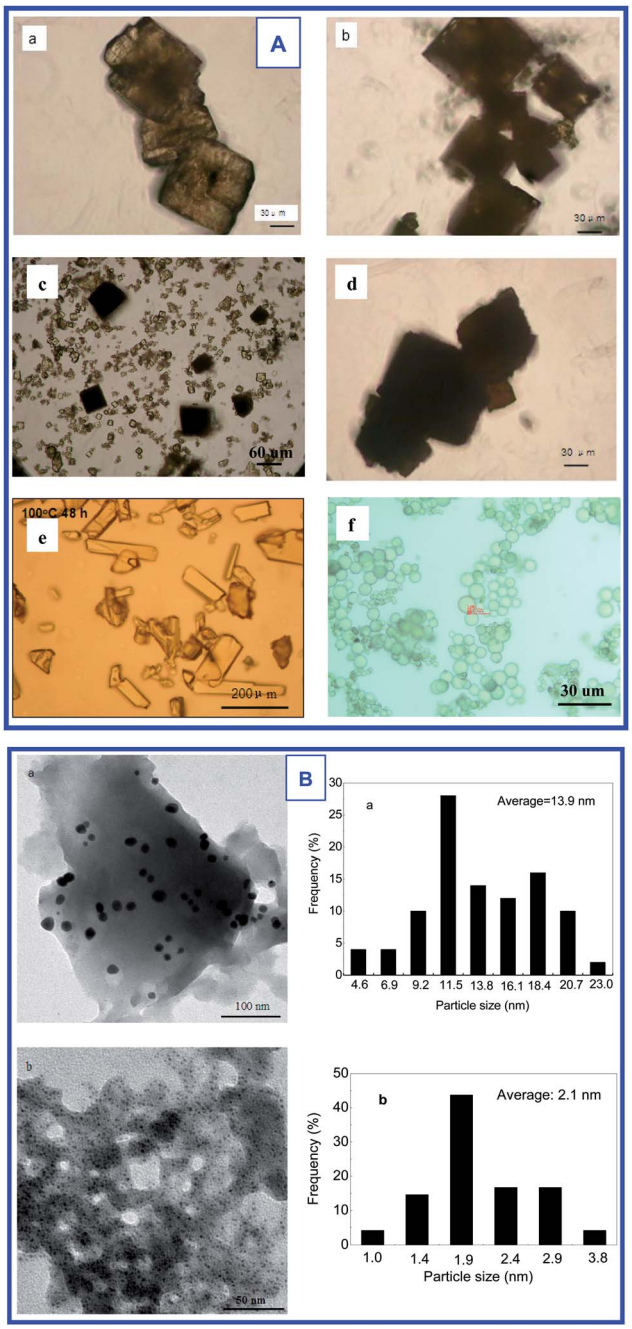

Fig. 1 (A) The optical microscope photograph of IRMOF-3 (a), IRMOF-3-Pr(OP) (b), IRMOF-3-Pr′(OP) (c), IRMOF-3–Pr(PM) (d), CUP-1 (e), and CUP-1–Pr(OP) (f); (B) TEM images and gold size distributions of Au/CUP-1(PM) (a) and Au/CUP-1(OP) (b) samples.

Au/CUP-1(PM) after the A^3 coupling reaction at 120 °C for 12 h sharply decreased despite of retaining the main diffraction peaks. No significant diffractions of gold crystal on Au/CUP-1(OP) are found due to the small gold size and low gold content (0.1%). The introduction of auxiliary chiral L-proline into the components of CUP-1 by OP method results in a sharp decrease of crystallinity, and only a weak peak at $2\theta = 6.8°$ is observed, indicating that the crystalline structure partially collapsed.

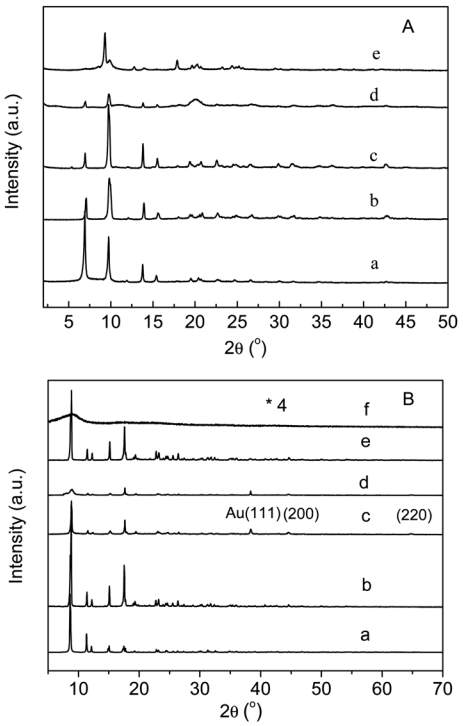

Fig. 2 (A) Powder XRD patterns of IRMOF-3 (a), IRMOF-3–Pr(OP) (b), IRMOF-3–Pr′(OP) (c), and IRMOF-3–Pr(PM) (d); (B) the simulated framework for CUP-1 (a), experiment measured CUP-1 (b), Au/CUP-1(PM) (c), Au/CUP-1(OP) (d), and CUP-1–Pr(OP) (e) samples.

3.4. Single-crystal XRD

Single-crystal XRD was carried out to determine exact crystalline structure of CUP-1 (see Tables S1–S3† of the ESI). X-ray crystallographic analysis reveals that CUP-1 crystallizes in the orthorhombic system, chiral space group $P2(1)2(1)2(1)$ with the formula of $Zn_2(atpt)(l\text{-}lac)(HCOO)$. Fig. 3 illustrates the section of the X-ray crystal structure of CUP-1. There are two unique zinc centers (Zn(1) and Zn(2)) in the polymeric structure, and both of them have a coordination number five and an uncommon trigonal-bipyramidal coordination environment as depicted in Fig. 3. The first Zn^{2+} ion is coordinated with a deprotonated

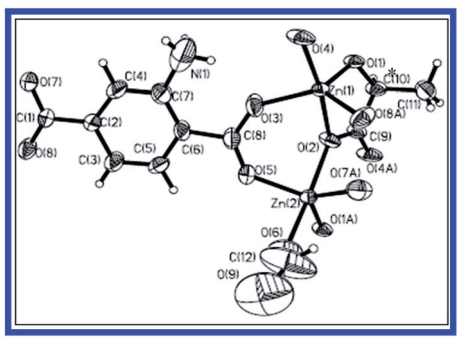

Fig. 3 Section of the X-ray crystal structure of CUP-1, showing the coordination environments of the Zn^{2+} ions and their connectivity with lactate anions. Thermal ellipsoids are set at 50% probability. The chiral C atom of the lactic ligand is marked by an asterisk.

hydroxy group of a lactate ligand, a carboxylate oxygen atom of 2-amino-1,4-benzenedicarboxylate ligand, and the oxygen atom of a formic ligand (the formic acids are generated by decomposition of DMF[35]) rather than DMF in the structure of **1**·DMF.[5] The second Zn^{2+} ion is chelated by one carboxylic oxygen atom of lactate ligand, and coordinated to a carboxylic oxygen atom of 2-amino-1,4-benzenedicarboxylate ligand. The chiral C atom (C(10)) of the lactic ligand is marked by an asterisk as shown in Fig. 3. In addition, the two Zn^{2+} ions are linked to each other by bridging carboxylate of H_2atpt ligand and one lactate ligand. And each lactate dianion connects four Zn^{2+} ions. In this structure, the Zn–Zn distance and Zn–O–Zn angles are 3.421 Å for Zn(1)–Zn(2), and 106.36° for Zn(2)–O(2)–Zn(1), respectively. The Zn–O bond lengths vary from 1.932 to 2.145 Å, and O–Zn–O angles vary from 79.34 to 171.5° (Tables S1 and S2†). Fig. 4 shows a view of the 1D chiral chains (A), projection in the (110) plane (B), and perspective view along *a* axis (C) in the structure of CUP-1. It can be seen that the Zn^{2+} ions and lactate ligands form 1D chiral chains running along the *a* axis. These chains act as secondary building units (SBUs), which are further interconnected by the benzene rings of 2-amino-1,4-benzenedicarboxylate in the other two directions to generate a 3D network with quadrangular channel dimensions of *ca.* 12 Å × 20 Å (measured between opposite atoms) viewed along the *a* axis. The chiral centers of the L-lactate moieties are exposed within the pores. In a word, the pores in CUP-1 have a homochiral environment.

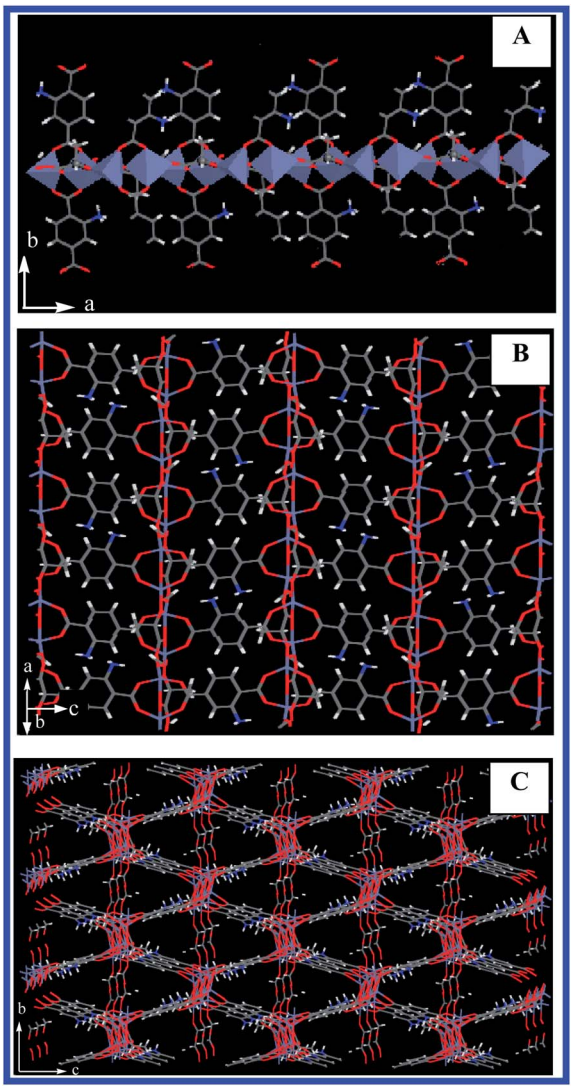

Fig. 4 A view of the 1D chiral chains (as both ball-and-stick/polyhedra and wire models; polyhedra represent the Zn coordination environments) in the structure of CUP-1 (A); projection of the structure of CUP-1 in the (110) plane (B); perspective view of the structure of CUP-1 along *a* axis (C). Note: the purple, red, blue, gray, and white represent Zn, O, N, C, and H atoms, respectively.

3.5. N_2 adsorption and desorption

Table 1 summarizes the data of surface area, pore size, and pore volume from N_2 adsorption–desorption at −196 °C for IRMOF-3, IRMOF-3–Pr(OP), IRMOF-3–Pr′(OP), and CUP-1 samples. In the present study, IRMOF-3 was synthesized by solvothermal with H_2atpt and $Zn(NO_3)_2 \cdot 6H_2O$ in DMF without N_2 protection. The surface area determined by BET and Langmuir equation is 1212 and 1468 $m^2\ g^{-1}$, respectively. This BET surface area is 62% higher than that (750 $m^2\ g^{-1}$) prepared by the "direct mixing" synthesis,[7] but it is still much lower than 2446 $m^2\ g^{-1}$ when using DEF as solvent.[36] We notice that different surface areas of IRMOF-3 have been reported.[7,10,33,34,36,37] The difference should be due to the different preparation conditions (*e.g.*, with/without N_2 protection, the different solvent employed). It was reported that higher BET surface area was obtained by using DEF rather than DMF as solvent.[10] The moisture adsorbed by MOFs upon exposure to ambient air and water residue in the reagent also affected the structure.[34] By introducing the auxiliary chiral L-proline into the components of IRMOF-3 with OP method, the surface area of IRMOF-3–Pr(OP) sharply decreased in comparison with IRMOF-3 (Table 1). The BET surface areas of IRMOF-3–Pr(OP) and IRMOF-3–Pr′(OP) are 140 and 166 $m^2\ g^{-1}$, respectively, which are *ca.* one eighth of IRMOF-3. It seems that the higher concentration of L-proline results in lower BET surface area. The BET and Langmuir surface area of CUP-1 is 78 and 104 $m^2\ g^{-1}$, respectively, which is only *ca.* one-tenth of IRMOF-3.

Fig. 5A shows the N_2 adsorption–desorption isotherms of IRMOF-3, IRMOF-3–Pr(OP), IRMOF-3–Pr′(OP) and CUP-1 samples. At first sight it seems that all samples feature the type IV isotherm with a hysteresis loop and thus possess mesopore, however, the adsorption isotherms exhibit a distinctive plateau so that adsorption volume approaches a limiting value as p/p_0 increasing from 0.009 to 0.90 for IRMOF-3, IRMOF-3–Pr(OP), and CUP-1 samples, which is a prominent feature of type I with microporous material. We also noted that the physisorption hysteresis in Fig. 5A includes type H2 for IRMOF-3–Pr′(OP) and type H1 for other samples. The pore diameters determined by BJH desorption method are 4.27, 3.75, 3.81, and 1.41 nm for IRMOF-3, IRMOF-3–Pr(OP), IRMOF-3–Pr′(OP) and CUP-1 samples, respectively (Table 1, Fig. S3†). The Saito–Foley (SF) method based on cylindrical pore geometry has been adopted to derive the microporous size distribution from physisorption

Table 1 Texture properties of IRMOF-3, IRMOF-3–Pr′(OP), and CUP-1 samples

	Surface area data ($m^2\ g^{-1}$)		Pore size data (nm)			Pore volume data ($cm^3\ g^{-1}$)		
Sample	BET	Langmuir	Average	Micro-[a]	Meso-[b]	Total[c]	Micro-[d]	Meso-[e]
IRMOF-3	1212	1468	2.56	0.97	4.27	0.77	0.51	0.40
IRMOF-3–Pr(OP)	140	188	2.86	0.69	3.75	0.10	0.07	0.05
IRMOF-3–Pr′(OP)	166	242	5.31	0.73	3.81	0.22	0.08	0.24
CUP-1	78	104	3.08	0.66	1.41	0.06	0.04	0.03

[a] Saito–Foley (SF) method pore diameter. [b] BJH method desorption pore diameter. [c] Total pore volume. [d] SF method cumulative pore volume. [e] BJH interpolated cumulative pore volume.

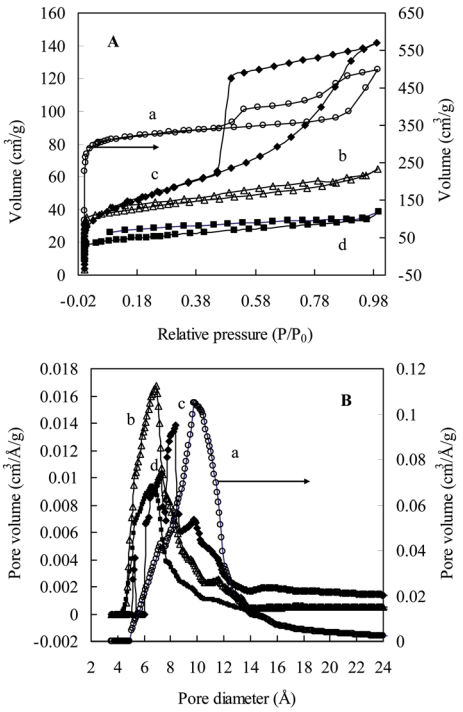

Fig. 5 N_2 adsorption–desorption isotherms (A) and pore diameter distribution determined by SF method (B) of IRMOF-3 (a), IRMOF-3–Pr(OP) (b), IRMOF-3–Pr′(OP) (c), and CUP-1 (d) samples.

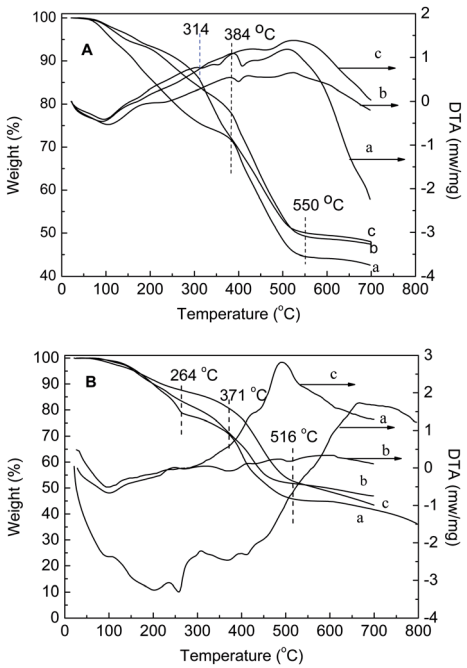

Fig. 6 (A) TG-DTA curves on IRMOF-3 (a), IRMOF-3–Pr(OP) (b), IRMOF-3–Pr(PM) (c); (B) TG-DTA curves on CUP-1 (a), CUP-1–Pr(OP) (b), and Au/CUP-1(OP) (c) samples.

isotherms as depicted in Fig. 5B. Clearly, the narrow microporous size distributions were found on IRMOF-3, IRMOF-3–Pr(OP), and CUP-1 samples, while a wider size distribution was observed on IRMOF-3–Pr′(OP). The microporous size diameters are 0.97, 0.69, 0.73, and 0.66 nm on IRMOF-3, IRMOF-3–Pr(OP), IRMOF-3–Pr′(OP), and CUP-1 samples, respectively.

3.6. Thermogravimetric and differential thermal analysis (TG-DTA)

TG-DTA experiment has been carried out to investigate the thermal stabilities of the IRMOF-3, CUP-1, and their modified samples. Fig. 6A shows the TG-DTA curves of IRMOF-3, IRMOF-3–Pr(OP) and IRMOF-3–Pr(PM) samples. The TG curves of all samples show two steps of weight loss stages in the temperature range from 25 to 700 °C. The first stage ranged from 40 to 384 °C corresponding to 29% and 22% of weight loss on IRMOF-3 and IRMOF-3–Pr(OP), respectively, was due to the release of physically adsorbed solvent molecules (*e.g.* $CHCl_3$ and DMF) and unreacted ligands (*e.g.* 2-aminoterephthalic), which was accompanied with an endothermic peak centered at *ca.* 100 °C in the DTA curve. The second stage ranged from 384 to 550 °C was due to the organic decomposition, which was accompanied with a broad exothermic peak centered at *ca.* 510 °C in the DTA curve. Notably, IRMOF-3–Pr(PM) started to decompose after *ca.* 314 °C. Clearly the thermal stability of IRMOF-3 and IRMOF-3–Pr(OP) samples was superior to that of IRMOF-3–Pr(PM). No plateau of weight loss was possibly due to too much physical adsorbed solvent remained on all the samples.

Fig. 6B shows the TG-DTA curves of CUP-1, CUP-1–Pr(OP) and Au/CUP-1(OP) samples. The weight loss of CUP-1 and Au/CUP-1(OP) samples could be divided into three stages with 40–264, 264–371, and 371–510 °C, corresponding to the desorption of physically adsorbed solvent molecules, further desorption of solvent and/or unreacted ligands within pores or on the surface

of the material, and the decomposition of the crystal structure, respectively. On the other hand the continuous loss of the weight was found on CUP-1–Pr(OP) until it was completely decomposed at 510 °C. It is evident that the thermal stability of CUP-1 and Au/CUP-1(OP) samples is much higher than that of CUP-1–Pr(OP).

3.7. Infrared spectrum (IR)

Fig. 7 shows IR spectra of IRMOF-3, IRMOF-3–Pr(OP), and IRMOF-3–Pr(PM) samples. The IR spectra of CUP-1, CUP-1–Pr(OP), Au/CUP-1(OP) and Au/CUP-1(PM) samples are given in Fig. 8. The IR spectra of IRMOF-3 show two peaks centered at 3473 and 3356 cm^{-1} due to the existence of the amino.[38] Whereas, these peaks become notably weak for IRMOF-3–Pr(PM), indicating the formation of amide by reaction of the NH_2 group of the H_2atpt ligand with carboxyl group of L-proline. However, it seems that the N–H stretches on IRMOF-3–Pr(OP) feature the same mode with IRMOF-3. This result could mean that NH_2 group of IRMOF-3–Pr(OP) is not transformed and the free L-proline should be encapsulated on the surface or pore. Notably the N–H stretches of CUP-1 red shift to 3458 and 3341 cm^{-1} in comparison with IRMOF-3, and these bands on CUP-1–Pr(OP) become weak, indicating that NH_2 group reacts with L-proline and transforms into amide. This result is in sharp contrast with L-proline functionalized IRMOF-3 by OP method. The N–H stretches were also observed on gold functionalized CUP-1 samples, the weak intensity could be due to nano gold particles deposited on their surface. The bands at 2926 cm^{-1} on all samples could be due to the stretching vibrations of the aromatic C–H. Specifically, the bands at 2973 and 2926 cm^{-1} on CUP-1 and its modified samples can be assigned to the vibrations of C–H originated from aromatic and/or formic ligand. The formic could be generated by decomposition of DMF.[35] For all samples, the two sharp bands at 1574 and 1382 cm^{-1} correspond to asymmetric (ν_{as}(C–O)) and symmetric (ν_s(C–O)) vibrations of carboxyl groups, respectively.[39] And the peaks centered at 1660, 1501, and 1432 cm^{-1} are ascribed to C=C stretching vibration of the aromatic. The 1253 cm^{-1} frequency can be assigned to C–N vibrations for all samples.

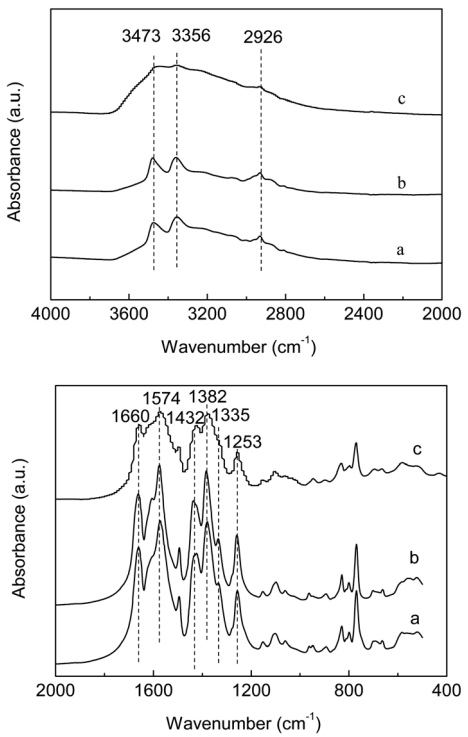

Fig. 7 Infrared spectra of IRMOF-3 (a), IRMOF-3–Pr(OP) (b), and IRMOF-3–Pr(PM) (c) samples.

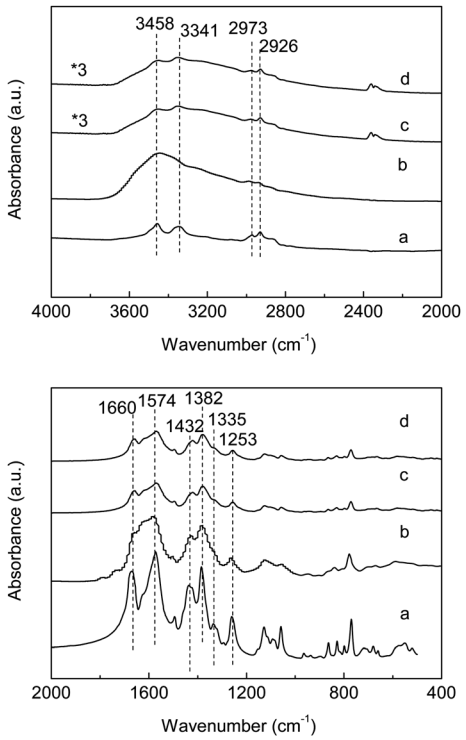

Fig. 8 Infrared spectra of CUP-1 (a), and CUP-1–Pr(OP) (b), Au/CUP-1(OP) (c), and Au/CUP-1(PM) (d) samples.

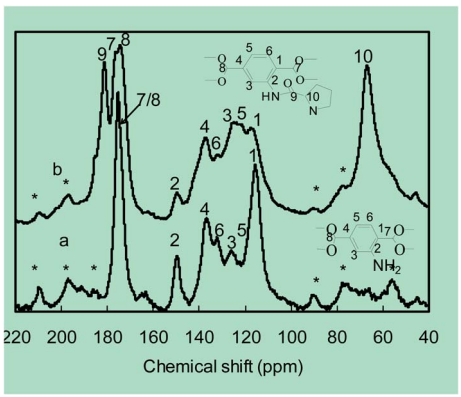

Fig. 9 Solid ^{13}C-NMR of IRMOF-3 (a) and IRMOF-3–Pr(PM) (b). The asterisks correspond to rotation bands.

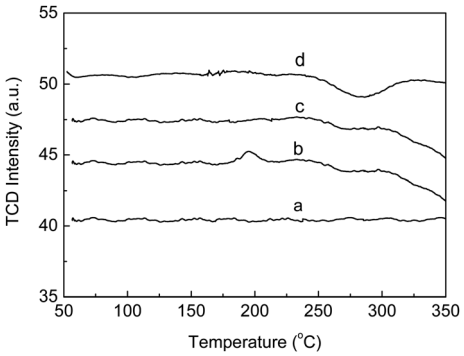

Fig. 10 TPR profiles of CUP-1 (a), Au/CUP-1(PM) (b), Au/CUP-1(PM) after reaction (c), and Au/CUP-1(OP) (d).

3.8. Solid state ^{13}C magic angle spinning nuclear magnetic resonance (MAS NMR)

Fig. 9 represents the solid state ^{13}C MAS NMR spectra of IRMOF-3 and IRMOF-3–Pr(PM). The ^{13}C resonance peaks at 174.8, 149.8 and 137.2–117.0 ppm of IRMOF-3 are assigned to O–C═O, phenylene C–NH_2, and the aromatic region, respectively. The post functionalization of L-proline for NH_2–Ph in IRMOF-3 has a significant effect upon the ^{13}C spectra. Of particular note is the decreased intensity of the resonance of the ring carbon with the attached amino group at 149.8 ppm. And the two carboxyl resonances are partially resolved. The additional resonances at 181.3 and 66.7 ppm on IRMOF-3–Pr(PM) compared with IRMOF-3 are assigned to the resonance signals of C═O of amide and N–CH, respectively (Fig. 9b). Spectral assignments of the aromatic ^{13}C resonances of IRMOF-3 are based on previous works.[7,40,41]

3.9. Temperature-programmed reduction (TPR)

TPR technique is usually used to quantitatively measure the reduction of oxidized gold species and thereby calculate the distribution of different gold oxidation states in supported Au catalysts.[30,42] Fig. 10 shows H_2-TPR profiles of CUP-1, Au/CUP-1(OP) and Au/CUP-1(PM) samples. The Au/CUP-1(PM) after one successive cycle of the A^3 coupling reaction is also included. The pristine CUP-1 and Au/CUP-1(OP) feature no hydrogen consumption in the range of 50–350 °C, indicating the gold species in Au/CUP-1(OP) should be metallic. However, one reduction peak centered at 196 °C was found on Au/CUP-1(PM), the reduction peak disappeared after the A^3 coupling reaction. The attempt to characterize the gold oxidation states of Au/CUP-1(PM) by X-ray photoelectron spectroscopy was failed due to the overlap of binding energies between Au 4f and Zn 3p. Zhang *et al.*[7] have previously observed two reduction peaks over IRMOF-3 immobilized gold catalyst prepared by PM method, and proposed that the reduction peak at *ca.* 239 °C was due to the reduction of Au^{3+}. We earlier prepared Au/IRMOF-3 using the similar method with Au/CUP-1(PM) and ascribed the peak ranged from 190 to 270 °C to the reduction of Au^{3+}.[30] Similar to the earlier works,[7,30] we presume that the low temperature peak

Table 2 Aldol reaction catalyzed by L-proline functionalized IRMOF-3 and CUP-1 catalysts[a]

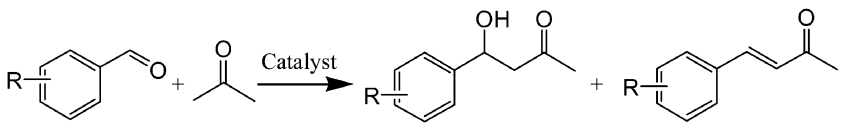

1 2

Entry	Catalyst	Aldehyde	T (°C)	t (h)	Conv. (%)	S_1[b] (%)	S_2[c] (%)	Y_1 (ee)[d] (%)	TON[e]
1	L-Proline	R = H	40	12	66	31	69	20 (12)	3
2[f]	L-Proline	R = H	r.t.	24	—	—	—	62 (60)	2
3[f]	L-Proline	R = 4-NO_2	r.t.	4	—	—	—	68 (76)	2
4	IRMOF-3	R = H	60	72	22	54	46	12 (0)	—
5	CUP-1	R = H	60	20	1	66	34	<1 (n.d.)	—
6	CUP-1–Pr(OP)	R = H	60	5	49	4	96	2 (n.d.)	3
7	IRMOF-3–Pr(OP)	R = H	r.t.	96	15	55	45	8 (98)	4
8	IRMOF-3–Pr(OP)	R = H	40	96	47	48	53	23 (73)	12
9	IRMOF-3–Pr(OP)	R = H	60	72	58	44	56	26 (10)	15
10	IRMOF-3–Pr(OP)	R = 4-NO_2	60	72	41	28	72	11 (89)	11
11	IRMOF-3–Pr(OP)	R = 3-Cl	60	30	50	23	77	11 (88)	13
12	IRMOF-3–Pr(OP)	*n*-Octaldehyde	60	120	66	33	67	22 (28)	17
13	IRMOF-3–Pr(OP)	Cyclohexane-carboxaldehyde	60	96	36	63	38	23 (52)	9
14	IRMOF-3–Pr(PM)	R = H	r.t.	180	34	35	65	12 (93)	6
15	IRMOF-3–Pr(PM)	R = H	40	96	57	31	69	18 (33)	10

[a] Reaction condition: IRMOF-3, IRMOF-3–Pr(OP) and IRMOF-3–Pr(PM): 20 mg; CUP-1–Pr(PM) and CUP-1–Pr(OP) 60 mg; L-proline 7.0 mg (0.06 mmol); benzaldehyde: 0.3 mmol. The molar ratio of benzaldehyde : acetone was 1 : 10, solvent: DMSO 0.5 g (6.4 mmol). [b] The selectivity of β-hydroxy carbonyl compound (**1**). [c] The selectivity of β-unsaturated carbonyl compound (**2**). [d] The yield of β-hydroxy carbonyl compound (**1**), the data in the parentheses are ee values which were determined by HPLC analyses (Chiralpack ID) with hexane/isopropanol as the eluent. The absolute configuration was not determined, n.d., not determined. [e] Calculated on the basis of L-proline. [f] Data from the ref. 31, the reaction conditions: 30% mmol proline, 0.1 mmol aldehyde, acetone–DMSO = 1/4 (v/v), acetone 0.2 mL.

is due to the reduction of Au^{3+} ions into Au^0 atoms, and the ratio of Au^{3+}/Au^0 in Au/CUP-1(PM) is 2.0.

3.10. Catalytic performance test

3.10.1 Asymmetric aldol reaction of aldehyde and acetone. Table 2 summarizes the catalytic performance of L-proline functionalized IRMOF-3 and CUP-1 catalysts for the aldol reaction. Reacting aldehyde with acetone on L-proline functionalized IRMOF-3 and CUP-1 catalysts affords the aldol products including β-hydroxy carbonyl compound (**1**) and α,β-unsaturated carbonyl compound (**2**). The product **2** is obtained by the dehydration of product **1**, and the two products are demonstrated by GC-MS analysis (Fig. S4†). The experiments of screening solvents (neat, DMF and DMSO) using the representative model reaction consisting of benzaldehyde and acetone showed that DMSO was a suitable solvent (Table S4†). Reacting benzaldehyde with acetone on the reference homogeneous L-proline at 40 °C addresses products **1** and **2** with selectivity of 31% and 69%, respectively, under the present reaction conditions. The yield of **1** is 20% with 12% ee (entry 1). List *et al.*[31] obtained the yield of 62%, 68% with 60% and 76% ee, respectively, in the case of benzaldehyde and 4-nitrobenzaldehyde as the substrate (entries 2 and 3). The reaction catalyzed by IRMOF-3 produces the products **1** and **2** with the selectivity of 54%, 46%, respectively, at 22% of benzaldehyde conversion (entry 4), while a control experiment with unmodified CUP-1 fails to give significant conversion (entry 5). Notably, the reaction catalyzed by CUP-1–Pr(OP) gives a significant conversion (49%) and high selectivity (96%) to **2** (entry 6). By introducing L-proline on IRMOF-3 by OP method, the benzaldehyde conversion of IRMOF-3–Pr(OP) decreases a little compared with L-proline; however, the benzaldehyde conversion is significantly enhanced compared with IRMOF-3 (entry 9 *vs.* 4). We note that a moderate conversion (58%) at 60 °C and 26% yield for **1** on IRMOF-3–Pr(OP), however, the ee is only 10% (entry 9). By decreasing the reaction temperature, the ee is sharply increased. Specifically, 98% ee with 8% yield can be obtained on IRMOF-3–Pr(OP) at room temperature (entry 7). The aryl aldehydes possessing electron withdrawing groups afford **1** with an enhanced ee (entries 10 and 11) over IRMOF-3–Pr(OP) catalyst at 60 °C compared with benzaldehyde. The reaction with aliphatic aldehyde like cyclohexanecarboxaldehyde also displays a moderate enantioselectivity, while the reaction with *n*-octaldehyde shows low ee on IRMOF-3–Pr(OP) catalyst (entries 12, and 13). Notably, reacting benzaldehyde with acetone on IRMOF-3–Pr(PM) at room temperature affords an excellent enantioselectivity (93%) with 12% yield of **1** (entry 14). The yield increases to 18%, whereas, the ee sharply decreases to 33% at 40 °C (entry 15).

By changing the reaction conditions, the catalytic performance of IRMOF-3–Pr(OP) for the aldol reaction can be significantly enhanced. As evidenced in Fig. 11, by increasing the amounts of catalyst (60 mg) and DMSO (1.0 g), the mole ratio of acetone/benzaldehyde (20), and by shortening the reaction time (24 h), the benzaldehyde conversion and the selectivity to **1** increased from 47% to 90%. The **1** yield was sharply enhanced from 23% to 78% while retaining the ee value of 73%.

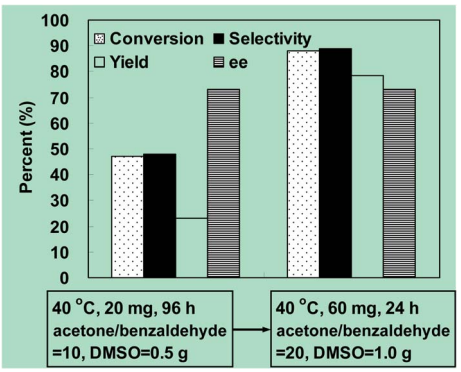

Fig. 11 Improve catalytic performance of IRMOF-3–Pr(OP) for the aldol reaction by optimizing the reaction condition.

One prominent advantage of the heterogeneous functionalized IRMOF-3 catalysts is their easy separation and recyclability. After the second successive cycles with intermediate extensive washing with DMSO, the catalytical activity of IRMOF-3–Pr(OP) and IRMOF-3–Pr(PM) decreases by around 30%. The further recycling however featured much less decrease (<10%) in activity.

3.10.2 The A^3 coupling reaction. The development of heterogeneous catalysts for preparing propargylamines by the A^3 coupling reaction remains an active research area.[27,42,43] Table 3 summarizes the A^3 coupling reaction catalyzed by gold functionalized CUP-1 catalysts. Gold functionalized CUP-1 catalysts feature 100% selectivity to the product of propargylamine for the reaction. Effect of reaction temperature on the yield of propargylamine over Au/CUP-1(PM) was explored (Table 3, entries 1–5). No higher than 17% yield of propargylamine was found at the reaction temperature less than 80 °C. A moderate yield (51%) is obtained at 100 °C, and a good yield (89%) can be obtained at 120 °C. We have analyzed the enantioselectivity for the propargylamine. The ee values are 6% and 4% with benzaldehyde at 100 and 120 °C, respectively (entries 4 and 5). The high reaction temperature (>100 °C) of the A^3 coupling reaction on Au/CUP-1(PM) catalyst offers no advantage for the ee. Aromatic aldehydes including those bearing functional groups such as alkyl and chloro are able to undergo the corresponding three-component-coupling at 120 °C, and afford good to excellent yields (entries 6 and 7). Aliphatic aldehydes such as *n*-octaldehyde and cyclohexanecarboxaldehyde also display good to excellent yields (entries 8 and 9). The A^3 coupling reaction with alicyclic amines such as piperidine, pyrrolidine, and morpholine proceeds smoothly to afford the corresponding propargylamines (entries 5, 10 and 11). Au/CUP-1(OP) with 0.1 wt% gold affords 5% yield at 120 °C, however, the turnover number (TON) calculated based on the gold weight is up to 35 (entry 12). The yield (79%) and TON (556) over Au/CUP-1(OP) can be remarkably enhanced by increasing the reaction temperature from 120 to 150 °C (entry 13).

Fig. 12 shows the reusability of Au/CUP-1(PM) and Au/CUP-1(OP) catalysts for the A^3 coupling reaction at 120 and 150 °C, respectively. The benzaldehyde conversion is 90% within 4 h at 120 °C over the fresh Au/CUP-1(PM) catalyst. After three

Table 3 Coupling of aldehyde, alkyne, and amine catalyzed by gold functionalized CUP-1 catalysts[a]

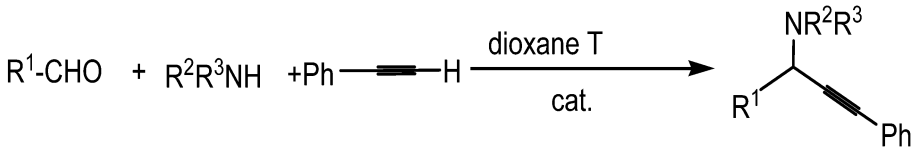

Entry	Catalyst	R^1	R^2R^3NH	T^b (h)	T (°C)	Yield (ee)[c] (%)	TON
1	Au/CUP-1(PM)	Ph	Piperidine	6	40	2	—
2	Au/CUP-1(PM)	Ph	Piperidine	5	60	4	—
3	Au/CUP-1(PM)	Ph	Piperidine	4	80	17	3
4	Au/CUP-1(PM)	Ph	Piperidine	12	100	51 (6)	8
5	Au/CUP-1(PM)	Ph	Piperidine	4	120	89 (4)	14
6	Au/CUP-1(PM)	4-$CH_3C_6H_4$	Piperidine	12	120	91	14
7	Au/CUP-1(PM)	3-ClC_6H_4	Piperidine	12	120	89	14
8	Au/CUP-1(PM)	Heptyl	Piperidine	12	120	79	12
9	Au/CUP-1(PM)	Cyclohexyl	Piperidine	12	120	97	15
10	Au/CUP-1(PM)	Ph	Pyrrolidine	12	120	81	13
11	Au/CUP-1(PM)	Ph	Morpholine	12	120	84	13
12	Au/CUP-1(OP)	Ph	Piperidine	4	120	5	35
13	Au/CUP-1(OP)	Ph	Piperidine	21	150	79	556

[a] Reaction conditions: aldehyde (0.250 mmol), amine (0.300 mmol), alkyne (0.325 mmol), catalyst (0.07 g, Au/CUP-1(PM): 6.42 mol%, Au/CUP-1(OP): 0.14 mol%). [b] The reaction time was not optimized. [c] The data in the parentheses are ee values determined by HPLC with a Chiralcel OD column, using hexane–ethanol (95/5) as a mobile phase.

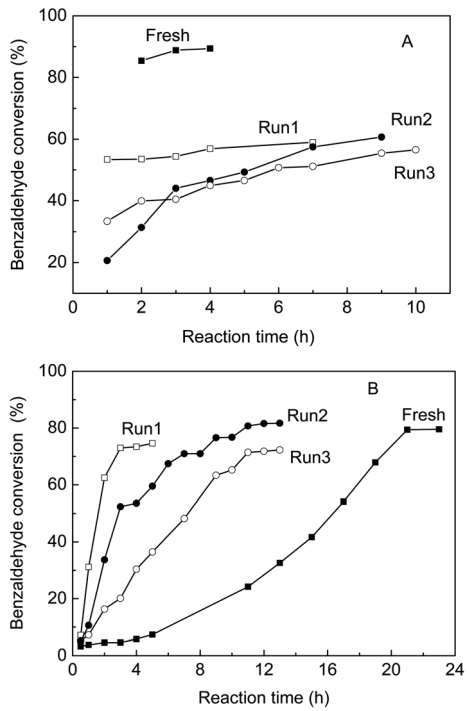

Fig. 12 The reusability of Au/CUP-1(PM) at 120 °C (A) and Au/CUP-1(OP) at 150 °C (B) for the A^3 coupling reaction.

successive cycles with intermediate extensive washing with 1,4-dioxane, the conversions were 59%, 61%, and 57% at the reaction time of 7, 9, and 10 h, respectively. Au/CUP-1(PM) features a significant deactivation by around 33% for the first run, while further recycling leads to very slight deactivation. The fresh Au/CUP-1(OP) exhibits an induction period for *ca.* 20 h. The maximum conversion (79%) is found at 150 °C within 21 h. The conversions are 75%, 82%, and 72% at the reaction time of 5, 13, and 13 h, respectively for the three successive runs. Clearly, no significant deactivation is found on Au/CUP-1(OP) catalyst.

4. Discussion

4.1. Prominent features of CUP-1 and IRMOF-3

Novel chiral MOFs could be synthesized by using a chiral ligand during the hydrothermal process or switching a preassembled achiral framework by PM with chiral catalytic units.[3,5,25] In this work we have successfully prepared a homochiral MOF denoted CUP-1 by using a mixture of chiral L-lactic acid and achiral H_2atpt ligands with conventional hydrothermal synthesis. The structure of CUP-1 is similar to that of **1**·DMF which was obtained by hydrothermal reaction of a mixture of $Zn(NO_3)_2$, L-lactic acid, and 1,4-benzenedicarboxylic acid (H_2bdc) in a mole ratio of 2 : 1 : 1 at 110 °C for 2 days.[5] The prominent advantage of CUP-1 over **1**·DMF is that the 2-amino group of the H_2atpt acid does not participate in coordination to the pentanuclear Zn nodes that link the structure together, and is potentially available for undergoing a variety of organic transformations as already demonstrated by IRMOF-3.[7,26–29]

As mentioned earlier, the IRMOF-3 containing NH_2–BDC as a building block was recently shown to undergo chemical modification with a diverse series of anhydrides, isocyanates and salicylaldehyde by PM strategy.[7,26–29] The PM strategy potentially provides a simple, efficient, and versatile route to synthesize numerous catalytically active chiral MOFs from a robust achiral

MOF for a variety of asymmetrical transformations, however, as commented by Yoon *et al.* in a recent review[6] that no example by introducing of organocatalytic units on the organic strut of preassembled framework with the PM strategy in asymmetrical transformations has been reported yet. By virtue of free NH_2 group in the frameworks of CUP-1 and IRMOF-3, we have explored L-proline functionalized IRMOF-3 and CUP-1 catalysts by PM and OP strategies for asymmetrical catalyzing aldol reaction of aldehyde with acetone. Considering creating metal ions/nanoparticles in MOFs representing another important class of MOF catalyst, we used the OP and PM strategies to introduce catalytic active sites of gold nanoparticles in the CUP-1.

4.2. Physicochemical properties of proline and gold functionalized CUP-1 and IRMOF-3 catalysts

The L-proline functionalized IRMOF-3 samples by OP method retain the crystalline integrity from the XRD analysis, while the IRMOF-3–Pr(PM) sample by PM method features some structure change of crystal (Fig. 2A). The differences in peak ratios at $2\theta = 6.8, 9.6^\circ$ between IRMOF-3–Pr(OP) and IRMOF-3 would mean that some unreacted linker/solvent was still present in the pores of IRMOF-3–Pr(OP), leading to the block, deviation or shrinkage of the pore in crystalline structure. We noted that IRMOF-3 modified with anhydrides by PM method also affected the intensity ratio for the typical two peaks (see Fig. 4 in ref. 27 and Fig. 3 in ref. 29). This assumption could be supported by the sharp decrease of the BET and Langmuir surface area for IRMOF-3–Pr(OP) and IRMOF-3–Pr′(OP) samples (Table 1).

It is well known that IRMOF-3 is microporous material, however, a well-defined type IV with a hysteresis, which is a prominent feature for mesoporous materials, is found on IRMOF-3, as well as CUP-1 (Fig. 5A). The mesoporosity should be attributed to the secondary particle piled pore, which comes from the aggregation of nanocrystals. This has been previously reported for materials synthesized in DMF under microwave irradiation, the so-called metal–organic gels.[44] The aggregation of nanocrystals was observed on IRMOF-3, CUP-1, and their modified samples by optical microscope photograph (Fig. 1A).

The IR results are commonly employed to distinguish the coordination modes of the carboxylate groups. A correlation of the carboxylate coordination mode to metal ions is usually made by examining the difference $\Delta\nu(\mathrm{COO}) = \nu_{as}(\mathrm{COO}) - \nu_s(\mathrm{COO})$ of the compound.[45] Clearly, the asymmetric ($\nu_{as}(\mathrm{COO})$) and symmetric ($\nu_s(\mathrm{COO})$) vibrations of carboxylate groups on all samples appeared at 1574 and 1382 cm^{-1}, respectively (Fig. 7 and 8). The value of $\Delta\nu(\mathrm{COO})$ is 192 cm^{-1} which is less than 200 cm^{-1}, indicating the bis-chelation of the carboxylic groups to the metal ion. These results are in accordance with the single-crystal X-ray analysis of IRMOF-3 and CUP-1. The absence of IR spectra at 1730 cm^{-1} which is ascribed to a stretching of protonated carboxylic group,[46] can be further in support that all the carboxylate groups of the H_2atpt ligand are completely deprotonated on all samples.

The new stretches of amide I (1695–1610 cm^{-1}) and amide II (1552–1520 cm^{-1})[47] could be overlapped by the stretches of aromatic (1625–1575 cm^{-1}, 1525–1475 cm^{-1}) for the FTIR of IRMOF-3–Pr(PM). Considering that the decrease of N–H stretches at 3473 and 3356 cm^{-1} associated with the amine of the H_2atpt ligand for FTIR of IRMOF-3–Pr(PM) could be due to the low-resolution spectrum or more water adsorbed, the solid ^{13}C MAS NMR was employed to characterize the amide bond. The decrease of resonance at 149.8 ppm is informative revealing that post-functionalization of the amine-pending groups of IRMOF-3. The new ^{13}C NMR band at 181.3 ppm attributed to the resonance signals of C=O of amide is in strong support of formation of amide (Fig. 9). It should be pointed out that the ^{13}C spectral signals of our IRMOF-3 agree well with the previous works,[7,40] while the resonance signals of C=O of amide in IRMOF-3–Pr(PM) changed down-field (shifted to left) compared with that earlier reported.[48,49] Oh *et al.* have assigned ^{13}C NMR band at 176.0 ppm to the amide bond of poly(2-cyano-1,4-phenyleneterephthalamide).[48] Serrano *et al.* reported the signal of C=O of poly(ester amide)s was centered at *ca.* 168.0 ppm.[49] The difference should result from the C=O of amide in different molecular structures.

The thermodynamically stable amide bond is, in principle, formed when a carboxylic acid reacts with an amine with the release of water. The energy threshold of the ammonium carboxylate salt formation must, however, be overcome, and the activating reagents such as carbodiimides imidazolium and phosphonium salts are employed. Direct amidation of carboxylic acids and amines occurs spontaneously under solvothermal conditions at high temperatures (>160 °C).[50] Therefore it seems difficult for the reaction between proline and the amine-pending group of IRMOF-3. The possibility of the amide formation in the IRMOF-3–Pr(PM) should be considered. Costa *et al.* have reported that the reaction of carboxylic acids (*e.g.*, acetic acid) with the amine-pending groups of MOF-LIC-1 without any activating reagents at 120 °C for 1 h led to formation of amide.[51] It was also reported that metallic Lewis acids, including heterogeneous Lewis acidic materials, and early transition metal complexes, like titanium(IV) species, have been employed as mediators or catalysts for the amidation reaction.[51,52] We presume that transition metal-containing MOFs (*e.g.* MOF-LIC-1 and IRMOF-3) may act as the catalysts for the amidation reaction. IRMOF-3 and aminofunctionalized MIL-53 are reported the stable solid basic catalysts in the Knoevenagel condensation of ethyl cyanoacetate and ethyl acetoacetate with benzaldehyde.[10] It is possible that a small amount of proline functionalized with IRMOF-3 by the PM method.

A surprising discovery made by Kim and coworkers has recently disclosed that ligand exchange can even occur with the inert Zr(IV)-based UiO-66 MOFs at room temperature.[53] The ligands including NH_2-BDC, 2-bromo-1,4-benzenedicarboxylate (Br-BDC), 2-azido-1,4-benzenedicarboxylate (N_3-BDC), 2-hydroxy-1,4-benzenedicarboxylate (OH-BDC) and 2,5-dihydroxy-1,4-benzenedicarboxylate (2,5-$(OH)_2$-BDC) can occur between UiO-66 MOFs as monitored by aerosol time-of-flight mass spectrometry (ATOFMS). The detail of linker exchange could only be uncovered by a single-particle analysis method, *i.e.*, ATOFMS. We are not sure if there is linker exchange during the post-synthetic modification of IRMOF-3 with proline, due to no availability of the ATOFMS at present.

Combined the synthetic strategies with the characterization results, we suggest that IRMOF-3, CUP-1, and their modified samples could be well understood on the basis of models as depicted in Scheme 1. The free NH_2 group of the H_2atpt ligand in both CUP-1 and IRMOF-3 provides the possibility for modification with catalytical active sites. By functionalizing CUP-1 and IRMOF-3 with auxiliary chiral L-proline with OP method, different scenarios can be devised based on the results of N_2 adsorption desorption, XRD, IR, and NMR characterizations. Our powder XRD measurements show that the crystalline structure of IRMOF-3–Pr(OP) is the same with IRMOF-3 (Fig. 2A). The NH_2 group also keeps intact on the sample demonstrated by IR analysis (Fig. 7). These results show clearly that the chiral L-proline is solely encapsulated in the surface and/or pore of IRMOF-3–Pr(OP) (Scheme 1e). On the other hand, the crystalline structure was partly broken and the stretching vibrations of N–H of CUP-1–Pr(OP) were sharply weakened compared with CUP-1 (Fig. 2B, and 8). These results mean that NH_2 group has reacted with L-proline into amide as shown in Scheme 1f. Notably, by postsynthetic modification of IRMOF-3 with auxiliary chiral L-proline, the NH_2 group of IRMOF-3–Pr(PM) has also transformed with L-proline into amide as indicated by XRD, IR, and NMR analysis (Scheme 1c). For Au/CUP-1(PM) prepared by PM method, the catalyst contains both metallic gold nanoparticles and cationic Au^{3+} species as indicated by H_2-TPR analysis. The cationic Au^{3+} species could be stabilized by O, N and Cl atoms (Scheme 1d). In the case of Au/CUP-1(OP) prepared by OP method, only metallic gold nanoparticles were verified by the H_2-TPR (Scheme 1g).

4.3. Proline functionalized MOFs for the aldol reaction

Aldol reaction is a useful method for preparing β-hydroxy carbonyl compounds and has attracted a great deal of attention from synthetic organic chemists.[31,33,41,42] The catalytic asymmetric aldol reaction as a fundamental C–C bond forming reaction in chemistry and biology is a hot topic.[31] We observed that aryl aldehydes possessing electron withdrawing groups feature a much higher ee than benzaldehyde (entries 9–11, Table 2). This was in accordance with the earlier report by using homogenous L-proline for the aldol reaction.[31] At room temperature, both IRMOF-3–Pr(OP) and IRMOF-3–Pr(PM) show an excellent ee value (≥93%) (entries 7 and 14). IRMOF-3–Pr(OP) catalyst exhibits a much higher ee than IRMOF-3–Pr(PM) at 40 °C, however, both catalysts show much higher ee than the homogeneous L-proline under the present reaction conditions (entries 1, 8 and 15). The better ee in the heterogeneous L-proline functionalized IRMOF-3 catalysts than the homogeneous counterpart may originate from the restricted movement of the substrates in the well confined microporous system in combination with multiple chiral inductions.[5,25] And the well defined framework of crystalline structure of IRMOF-3–Pr(OP) than that of IRMOF-3–Pr(PM) could result a higher ee for the reaction.

Despite the good to excellent enantioselectivity on L-proline functionalized IRMOF-3 catalysts in most cases, the yield of β-hydroxy carbonyl compounds was below 30% (Table 2). List *et al.* first discovered that proline can efficiently catalyze asymmetric aldol reaction.[31] They obtained 68% yield and 76% ee in the reaction of acetone with 4-nitrobenzaldehyde, and 62% yield and 60% ee by using 30–40 mol% proline in the case of benzaldehyde (entries 2 and 3, Table 2). The much higher yield and ee than ours (20% yield and 12% ee, entry 1, Table 2) should be due to the larger amount of L-proline (30–40 mol%), acetone (acetone–aldehyde, mol mol^{-1} = 27), and DMSO solvent (DMSO–aldehyde = 113) compared with ours (20 mol%, acetone–aldehyde = 10, DMSO–aldehyde = 21). The higher amount of proline and acetone can certainly improve the conversion of aldehyde and the yield. The higher amounts of acetone and DMSO also significantly suppressed the side products. It should be pointed out that the significant side product of α,β-unsaturated carbonyl compound was found under the present reaction conditions. It is well known that the α,β-hydroxy carbonyl compound is not stable and can be facially condensed. The only significant side product (unsaturated ketone) was earlier observed by List *et al.*[31] As demonstrated by the earlier works,[25,31] L-proline and its derivatives are essentially the active sites for the asymmetric aldol reaction. Due to the low amounts of active sites in IRMOF-3–Pr(OP) (3.8 mol%) and IRMOF-3–Pr(PM) (9.2 mol%) catalysts under the present conditions, the yields are thus generally low. Notably the TON (4–17) calculated on the basis of L-proline on IRMOF-3–Pr(OP) and IRMOF-3–Pr(PM) are significantly higher than that of the homogeneous L-proline (2–3). Furthermore, the catalyst recovery and process work-up for the homogeneous L-proline are much difficult and the ee values in some cases are low. It is not then surprising that research efforts are being made today to bridge the gap between homogeneous and heterogeneous catalysis.

The low yields of β-hydroxy carbonyl compounds can be greatly enhanced by optimizing the reaction conditions. As shown in Fig. 11, by using thrice amount of IRMOF-3–Pr(OP) and suppressing the side-product with increasing the amounts of acetone and DMSO, and shortening the reaction time, the yield of **1** is increased significantly from 23% to 78%. And the TON number is 8. Banerjee and coworkers[25] introduced L-proline derivatives into the metal nodes of MIL-101 with PM method which contained very high concentration of active groups. The high yield (up to 91%) of β-hydroxy carbonyl compound was reported, however, the TON calculated on the basis of the active L-proline derivatives was only *ca.* 5. Lun *et al.*[18] incorporated proline protected by Boc groups into MOFs by presynthesis. And then the Boc groups were unveiled by a simple postsynthetic heating step. The resulted IRMOF-Pro was evaluated for asymmetrical aldol reaction of 4-nitrobenzaldehyde with acetone. Although the complete consumption of 4-nitrobenzaldehyde was deduced by TLC within 24 h, the ee of aldol product was determined to be 29% by chiral HPLC analysis. Wu *et al.* explored the aldol reaction between aldehydes and cyclohexanone on pyrrolidine based ligands (BCIP) incorporated MOFs. Moderate ee values (*ca.* 60%) were observed.[54]

Considering in the synthesis of IRMOF-3–Pr(PM) catalyst, there was no wash step for removing un-reacted L-proline. The leach of un-reacted and un-bounded L-proline should be responsible for the deactivation of the first recycled IRMOF-3–

Pr(PM) and IRMOF-3–Pr(OP) catalysts during the aldol reaction. The leach of proline was however sharply decreased evidenced by GC analysis during the further recycling.

4.4. Catalytic performance of MOFs catalysts for the A^3 coupling reaction

The marriage between catalytically active metal ions/clusters and MOFs could bridge the gap between homogeneous and heterogeneous catalysts.[4,7–9,55] Wei and Li[56] have initially reported that the A^3 coupling reaction catalyzed by homogeneous gold catalysts (*e.g.* $AuBr_3$). The silver, copper, and mercury salts were also found to be able to catalyze the reaction. The homogeneous gold salts were reported to endow the highest catalytic activity.[57–59] However, the limitations and the deactivation for homogenous gold salts make it impossible for sustainable catalytic process. Our Au/CUP-1(PM) catalyst showed good to excellent yields of propargylamine for the A^3 coupling reaction at 120 °C. And the catalyst can be applied to various aldehydes (including aromatic and aliphatic aldehydes), as well as amines (piperidine, pyrrolidine and morpholine). The good yield can be also achieved with the highest TON (556) on Au/CUP-1(OP) catalyst at 150 °C (Table 3). Since the size of gold nanoparticles on Au/CUP-1(PM) and Au/CUP-1(OP) catalysts is clearly much larger than that of the average pore size of CUP-1, the gold nanoparticles should be deposited on the surface of CUP-1. Therefore the A^3 coupling reactions occur on the surface of CUP-1. Compared with the other heterogeneous catalysts for the A^3 coupling reaction, our gold functionalized CUP-1 catalysts showed higher TON numbers than that of unsupported gold nanoparticles (TON: *ca.* 9),[60] and comparable activity with the earlier reported Au/IRMOF-3 catalysts.[30] Specifically, the TON numbers on Au/CUP-1(OP) catalyst at 150 °C is much higher than that of gold on layered double hydroxide (*ca.* 30)[61] and gold supported on commercial nano active magnesium oxide (*ca.* 407).[62] In particular, the gold functionalized CUP-1 catalysts show a good stability and can be reused at least 4 times. The excellent performances for catalyst reuse shed the advantage of using MOFs as stabilizers.

The high catalytic performance for the A^3 coupling reaction should be due to CUP-1 immobilized gold nanoparticles. The relatively high surface area and the free NH_2 groups of the CUP-1 can stabilize the gold nanoparticles. The alkyne was activated by the CUP-1 immobilized gold nanoparticles and transformed into the alkenyl–Au intermediate, which then reacted with the iminium ion generated *in situ* from the aldehydes and secondary amines to give the corresponding propargylamines.[30,43,57] As it was well established that cationic gold species showed higher catalytic activity than that of metallic gold counterpart for the A^3 coupling reaction,[43,56] we presume that the deactivation of Au/CUP-1(PM) in the first recycle could be due to the reduction of Au^{3+} into metallic atoms as demonstrated by the TPR analysis (Fig. 10). Moreover, we didn't wash the catalyst in the synthesis of Au/CUP-1(PM). It is possible that un-reacted gold precursor remained in the Au/CUP-1(PM). The leach of gold precursor could be another reason for the deactivation in the A^3 coupling reaction. It should be pointed out that there is a slight leaching of gold (*ca.* 10%) over Au/CUP-1(PM) after each recycle, however, much lower amount (<5%) of gold leaching is found on Au/CUP-1(OP), which is in accordance with our earlier finding that the catalyst prepared with OP strategy has much higher stability than that prepared with PM strategy.[30]

5. Conclusion

In summary, a novel homochiral Zn-containing MOF referred to as CUP-1 was successfully prepared based on the reaction of the mixed linkers of H_2atpt and L-lactic acids in a OP synthesis. CUP-1 crystallizes in the orthorhombic system, chiral space group $P2(1)2(1)2(1)$ with the formula of Zn_2(atpt)(l-lac)(HCOO). By virtue of free NH_2 group in the frameworks of CUP-1 and IRMOF-3, the catalytically active chiral L-proline or gold was chosen to modify the CUP-1 and/or IRMOF-3 catalysts by OP and PM strategies. The L-proline functionalized IRMOF-3 catalysts showed fair to excellent enantioselectivity (up to 98%) in asymmetrical aldol reactions with a higher TON and catalytic stabilities than the homogeneous counterpart of L-proline. By increasing the amounts of catalyst, acetone and DMSO, and shorten the reaction time, the yield of desired β-hydroxy carbonyl compound can be significantly enhanced while the by-product α,β-unsaturated carbonyl compound can be greatly suppressed. The gold functionalized CUP-1 by PM method contain a mixture of Au^0 and Au^{3+}, while the catalyst prepared with OP method contained ultrafine metallic gold nanoparticles with averaged size of *ca.* 2.1 nm. The gold functionalized CUP-1 catalysts showed high activity, selectivity (100% for propargylamines), and reusability (3 recycles) for the A^3 coupling reaction, despite the significant aggregation of the gold nanoparticles during the recycle runs. This work provides general methods to functionalize MOFs with the active ligand and metal nanoparticles for fabrication of highly efficient MOF-based heterogeneous catalysts.

Acknowledgements

We thank the National Natural Science Foundation of China (no. 20903119, 21173269, and 91127040) and National Key Technology R & D Program (grant: 2011BAK15B05) of China.

References

1 A. Corma, *Catal. Rev.: Sci. Eng.*, 2004, **46**, 369.
2 J. R. Long and O. M. Yaghi, *Chem. Soc. Rev.*, 2009, **38**, 1213.
3 Z. Wang, G. Chen and K. L. Ding, *Chem. Rev.*, 2009, **109**, 322.
4 L. Q. Ma, C. Abney and W. B. Lin, *Chem. Soc. Rev.*, 2009, **38**, 1248.
5 D. N. Dybtsev, A. L. Nuzhdin, H. Chun, K. P. Bryliakov, E. P. Talsi, V. P. Fedin and K. Kim, *Angew. Chem., Int. Ed.*, 2006, **45**, 916.
6 M. Yoon, R. Srirambalaji and K. Kim, *Chem. Rev.*, 2012, **112**, 1196.
7 X. Zhang, F. X. L. I. Xamena and A. Corma, *J. Catal.*, 2009, **265**, 155.

8 I. Luz, F. X. L. I. Xamena and A. Corma, *J. Catal.*, 2010, **276**, 134.
9 I. Luz, F. X. L. I. Xamena and A. Corma, *J. Catal.*, 2012, **285**, 285.
10 J. Gascon, U. Aktay, M. D. Hernandez-Alonso, G. P. M. Klink and F. Kapteijn, *J. Catal.*, 2009, **261**, 75.
11 J. Juan-Alcaniz, E. V. Ramos-Fernandez, U. Lafont, J. Gascon and F. Kapteijn, *J. Catal.*, 2010, **269**, 229.
12 P. Serra-Crespo, E. V. Ramos-Fernandez, J. Gascon and F. Kapteijn, *Chem. Mater.*, 2011, **23**, 2565.
13 E. V. Ramos-Fernandez, C. Pieters, B. Linden, J. Juan-Alcañiz, P. Serra-Crespo, M. W. G. M. Verhoeven, H. Niemantsverdriet, J. Gascon and F. Kapteijn, *J. Catal.*, 2012, **289**, 42.
14 S. Marx, W. Kleist and A. Baiker, *J. Catal.*, 2011, **281**, 76.
15 D. Jiang, T. Mallat, D. M. Meier, A. Urakawa and A. Baiker, *J. Catal.*, 2010, **270**, 26.
16 A. M. Shultz, O. K. Farha, D. Adhikari, A. A. Sarjeant, J. T. Hupp and S. T. Nguyen, *Inorg. Chem.*, 2011, **50**, 3174.
17 J. S. Seo, D. Whang, H. Lee, S. I. Jun, J. Oh, Y. J. Jeon and K. Kim, *Nature*, 2000, **404**, 982.
18 D. J. Lun, G. I. N. Waterhouse and S. G. Telfer, *J. Am. Chem. Soc.*, 2011, **133**, 5806.
19 R. K. Deshpande, J. L. Minnaar and S. G. Telfer, *Angew. Chem., Int. Ed.*, 2010, **49**, 4598.
20 M. J. Ingleson, J. Bacsa and M. J. Rosseinsky, *Chem. Commun.*, 2007, 3036.
21 C. D. Wu, A. Hu, L. Zhang and W. Lin, *J. Am. Chem. Soc.*, 2005, **127**, 8940.
22 C. Wu and W. Lin, *Angew. Chem., Int. Ed.*, 2007, **46**, 1075.
23 R. Vaidhyanathan, D. Bradshaw, J. N. Rebilly, J. P. Barrio, J. A. Gould, N. G. Berry and M. J. Rosseinsky, *Angew. Chem., Int. Ed.*, 2006, **45**, 6495.
24 M. J. Ingleson, J. P. Barrio, J. Bacsa, C. Dickinson, H. Park and M. J. Rosseinsky, *Chem. Commun.*, 2008, 1287.
25 M. Banerjee, S. Das, M. Yoon, H. J. Choi, M. H. Hyun, S. M. Park, G. Seo and K. Kim, *J. Am. Chem. Soc.*, 2009, **131**, 7524.
26 S. M. Cohen, *Chem. Rev.*, 2012, **112**, 970.
27 K. K. Tanabe, Z. Wang and S. M. Cohen, *J. Am. Chem. Soc.*, 2008, **130**, 8508.
28 M. J. Ingleson, J. P. Barrio, J. B. Guilbaud, Y. Z. Khimyak and M. J. Rosseinsky, *Chem. Commun.*, 2008, 2680.
29 Z. Wang and S. M. Cohen, *J. Am. Chem. Soc.*, 2007, **129**, 12368.
30 L. L. Liu, X. Zhang, J. S. Gao and C. M. Xu, *Green Chem.*, 2012, **14**, 1710.
31 B. List, R. A. Lerner and C. F. Barbas III, *J. Am. Chem. Soc.*, 2000, **122**, 2395.
32 N. Wolfgang, T. Fujie and C. F. Barbas III, *Acc. Chem. Res.*, 2004, **37**, 580.
33 M. Eddaoudi, J. Kim, N. Rosi, D. Vodak, J. Wachter, M. O'Keeffe and O. M. Yaghi, *Science*, 2002, **295**, 469.
34 J. G. Nguyen and S. M. Cohen, *J. Am. Chem. Soc.*, 2010, **132**, 4560.
35 J. H. He, Y. T. Zhang, Q. H. Pan, J. H. Yu, H. Ding and R. R. Xu, *Microporous Mesoporous Mater.*, 2006, **90**, 145.
36 J. L. C. Rowsell and O. M. Yaghi, *J. Am. Chem. Soc.*, 2006, **128**, 1304.
37 S. J. Wang, X. X. He, L. X. Song and Z. Y. Wang, *Synlett*, 2009, 447.
38 S. J. Garibay, Z. Q. Wang and S. M. Cohen, *Inorg. Chem.*, 2010, **49**, 8086.
39 J. H. He, Y. T. Zhang, J. H. Yu, Q. H. Pan and R. R. Xu, *Mater. Res. Bull.*, 2006, **41**, 925.
40 W. Morris, R. E. Taylor, C. Dybowski, O. M. Yaghi and M. A. Garcia-Garibay, *J. Mol. Struct.*, 2011, **1004**, 94.
41 S. Antonijevic and N. Halpern-Manners, *Solid State Nucl. Magn. Reson.*, 2008, **33**, 82.
42 X. Zhang, Y. C. Guo, Z. Z. Zhang, J. S. Gao and C. M. Xu, *J. Catal.*, 2012, **292**, 213.
43 X. Zhang and A. Corma, *Angew. Chem., Int. Ed.*, 2008, **47**, 4358.
44 S. K. Nune, P. K. Thallapally and B. P. McGrail, *J. Mater. Chem.*, 2010, **20**, 7623.
45 K. Nakamoto, *Infrared and Raman Spectra of Inorganic and Coordination Compounds*, John Wiley and Sons, New York, 1997.
46 Z. L. Xie, M. L. Feng, J. R. Li and X. Y. Huang, *Inorg. Chem. Commun.*, 2008, 1143.
47 T. Miyazawa and E. R. Blout, *J. Am. Chem. Soc.*, 1961, **83**, 712.
48 T.-J. Oh, J.-H. Nam and Y. M. Jung, *Vib. Spectrosc.*, 2009, **51**, 15.
49 P. J. M. Serrano, J. P. M. van Duynhoven, R. J. Gaymans and R. Hulst, *Macromolecules*, 2002, **35**, 8013.
50 H. Lundberg, F. Tinnis and H. Adolfsson, *Chem.–Eur. J.*, 2012, **18**, 3822.
51 J. S. Costa, P. Gamez, C. A. Black, O. Roubeau, S. J. Teat and J. Reedijk, *Eur. J. Inorg. Chem.*, 2008, 1551.
52 M. Hosseini-Sarvari, E. Sodagar and M. M. Doroodmand, *J. Org. Chem.*, 2011, **76**, 2853.
53 M. Kim, J. F. Cahill, Y. Su, K. A. Prather and S. M. Cohen, *Chem. Sci.*, 2012, **3**, 126.
54 P. Wu, C. He, Z. Xie and C. Duan, *J. Am. Chem. Soc.*, 2010, **132**, 14321.
55 O. K. Farha, A. M. Shultz, A. A. Sarjeant, S. T. Nguyen and J. T. Hupp, *J. Am. Chem. Soc.*, 2011, **133**, 5652.
56 C. Wei and C. J. Li, *J. Am. Chem. Soc.*, 2003, **125**, 9584.
57 C. Wei, Z. Li and C. J. Li, *Org. Lett.*, 2003, **5**, 4473.
58 L. Shi, Y. Q. Tu, M. Wang, F. M. Zhang and C. A. Fan, *Org. Lett.*, 2004, **6**, 1001.
59 L. P. Hua and W. Lei, *Chin. J. Chem.*, 2005, **23**, 1076.
60 M. Kidwai, V. Bansal, A. Kumar and S. Mozumdar, *Green Chem.*, 2007, **9**, 742.
61 M. L. Kantam, B. V. Prakash, C. R. V. Reddy and B. Sreedhar, *Synlett*, 2005, 2329.
62 K. Layek, R. Chakravarti, M. L. Kantam, H. Maheswaran and A. Vinu, *Green Chem.*, 2011, **13**, 2878.